Chapter 1

Introduction

The atomic nucleus is the dense, positively charged core of an atom, composed primarily of protons and neutrons—collectively known as nucleons. These nucleons are held together by the strong nuclear force, which is much stronger than the electromagnetic force that causes like charges to repel each other. The protons and neutrons within the nucleus are tightly bound together. According to the shell model picture, these nucleons lie in different nucleonic orbits, each of which is characterized by certain quantum numbers, *e.g.* total angular momentum, parity, etc. The nuclei with proton and/or neutron numbers close to the spherical shell gaps at 2, 8, 20, 28, 50, 82, and 126 are mostly spherical in nature, while the nuclei with nucleon numbers away from these shell closures (mid-shell nuclei) are mostly deformed in nature [1]. In quantum physics, when a perfectly spherical system rotates, it appears identical from any direction, and there is no point of reference for identifying the change in position. In these nuclei, the angular momentum states are generated via the excitation of a few individual nucleons and/or the holes created as a result of the promotion of protons and/or neutrons into higher-lying orbits (commonly known as single-particle excitations [2]). A nucleus with a deformed shape can also have a collective mode of excitations in which all or several of the nucleons take part coherently in generating an excited state in the nucleus [3]. The rotational and vibrational bands of a deformed nucleus

are examples of nuclear collective excitation. The excitation energies of the rotational band follow the relation $E \propto I(I+1)$ pattern [4–7], where E and I are the excitation energy and total angular momentum of the nucleus, respectively. On the other hand, energy levels in vibrational nuclei are equidistant and follow the relation $n\hbar\omega$, where n = 0, 1, 2, ... are the number of phonons [8, 9].

In the case of deformed nuclei, the distribution of nucleons within the nucleus can be quite complex. Depending on the number of nucleons and the forces acting within the nucleus, a nucleus can have spherical, prolate (elongated), oblate (flattened), and triaxial shapes. The collective model defines the deformed shape by the surface coordinate R in the (θ, ϕ) as [10, 11]

$$R(\theta,\phi) = R_0[1 + \sum_{\lambda=0}^{\infty} \sum_{\mu=-\lambda}^{+\lambda} \alpha_{\lambda\mu} Y_{\lambda\mu}(\theta,\phi)] \tag{1.1}$$

Where R_0 is the radius of the spherical nucleus. The $\alpha_{\lambda\mu}$ represent the amplitude of the complete set of spherical harmonics $Y_{\lambda\mu}(\theta,\phi)$. The λ is the multipolarity of the shape oscillations (*e.g.*, λ = 0, 1, 2,.... terms correspond to the monopole, dipole, quadrupole, and higher order of modes respectively) and μ is the projection of λ. Monopole order (λ= 0) requires a huge amount of energy for the nuclear surface to shrink and is irrelevant to the study of shape oscillation. Similarly, for λ = 1, *i.e.*, the dipole mode, represents translation of the center of mass and hence is discarded. Thus, the lowest mode of interest is the quadrupole mode of excitation with λ = 2.

For $\lambda = 2$ term, the five coefficients of $\alpha_{2\mu}$ reduce to two real independent deformation parameters $a_{2,0}$ and $a_{2,2} = a_{2,-2}$ (for axially symmetric quadrupole deformation). These two parameters can be expressed in terms of Hill-Wheeler coordinates β and γ as [12]:

$$a_{2,0} = \beta\cos\gamma, \quad a_{2,2} = \frac{1}{\sqrt{2}}\beta\sin\gamma \tag{1.2}$$

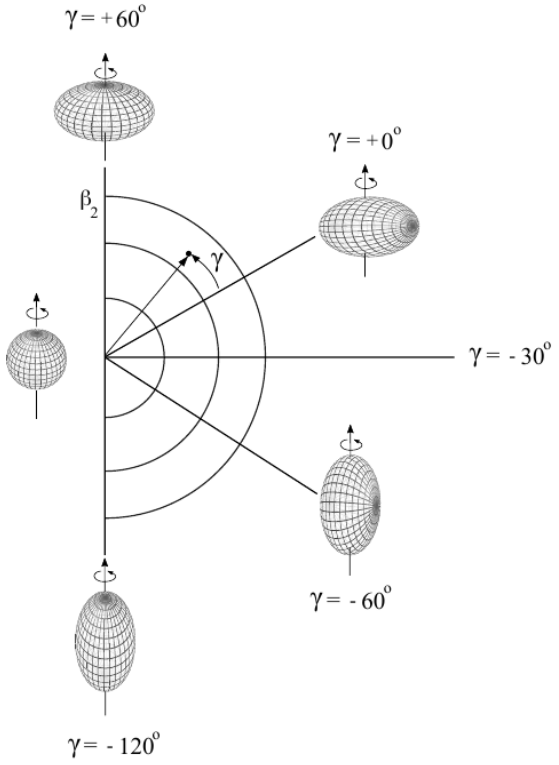

Figure 1.1 Schematic diagram of the shape parameters in rotating quadrupole-deformed nuclei [11].

β represents the degree of deformation, while the parameter γ gives the degree of axial asymmetry. The deformation of a nucleus can be visualized by the two deformation parameters β and γ. The increase in length $\Delta R = R(\theta,\phi) - R_0$ along the three body fixed axes can be represented as

$$\Delta R_k = R_0\sqrt{\frac{5}{4\pi}}\beta\cos\left(\gamma - \frac{2\pi}{k}k\right) \tag{1.3}$$

where k = 1, 2, 3. Two different axially symmetric shapes are possible for various orientations in space, viz.,

1. **Prolate shapes**: for $\gamma = 0^\circ, 120^\circ$, and $240^\circ (\beta > 0)$

2. **Oblate shapes**: for $\gamma = 60^\circ, 180^\circ$, and $300^\circ (\beta < 0)$

In Fig. 1.1 different nuclear shapes have been shown in the $\beta - \gamma$ plane for $\lambda = 2$. When $\beta > 0$, the nucleus has the elongated form of a prolate ellipsoid; when $\beta < 0$, the nucleus has the flattened form of an oblate ellipsoid. The interval $0^\circ \leq \gamma \leq 60^\circ$ is sufficient to describe all the quadrupole shapes due to discrete symmetries. The $\gamma = 0^\circ(-60^\circ)$ corresponds to collective prolate (collective oblate), while the $\gamma = 60^\circ(-120^\circ)$ describes non-collective oblate (non-collective prolate). If the γ value is not a multiple of 60°, then triaxial shapes emerge.

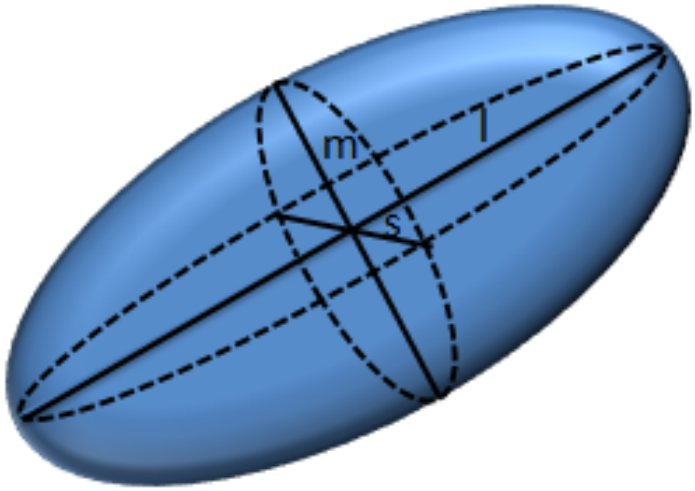

Figure 1.2 Pictorial representation of triaxial shape with three unequal axes.

In a triaxial nucleus Fig. 1.2, the shape lacks axial symmetry. Hence, the nucleus has three distinct axes, each with a different length. This deformation leads to unique nuclear properties and has implications for understanding nuclear reactions, stability, and the dynamics of nuclear processes.

The mass region $A \approx 120$ with 50 (spherical shape) $< Z <$ 57 (deformed shape) has been of much interest over the past few decades and is known to exhibit a variety of nuclear phenomena. Most of the stable Sn isotopes and their neighboring nuclei are near spherical and the low-lying excited states could be well explained by single particle excitations. The

nuclei away from the $Z = 50$ shell-closer region are deformed nuclei, and excited states in these nuclei are, therefore, generated by the collective motion of nucleons. The proton Fermi surface in these mass regions lies in the lower part of the $h_{11/2}$ orbitals, which favors prolate shape, whereas neutrons occupy medium- to high-Ω (Ω = projection of angular momentum of a nucleon on the symmetry axis.) orbitals of the $h_{11/2}$ subshell, which tries to drive the shape towards oblate. Excitation of nucleons into the $h_{11/2}$ deformation-driving orbitals can cause shape change, including triaxiality. When $h_{11/2}$ protons align due to rotation-induced Coriolis effects, nuclei are driven towards a prolate shape, whereas $h_{11/2}$ neutrons get aligned, an oblate shape is favored.

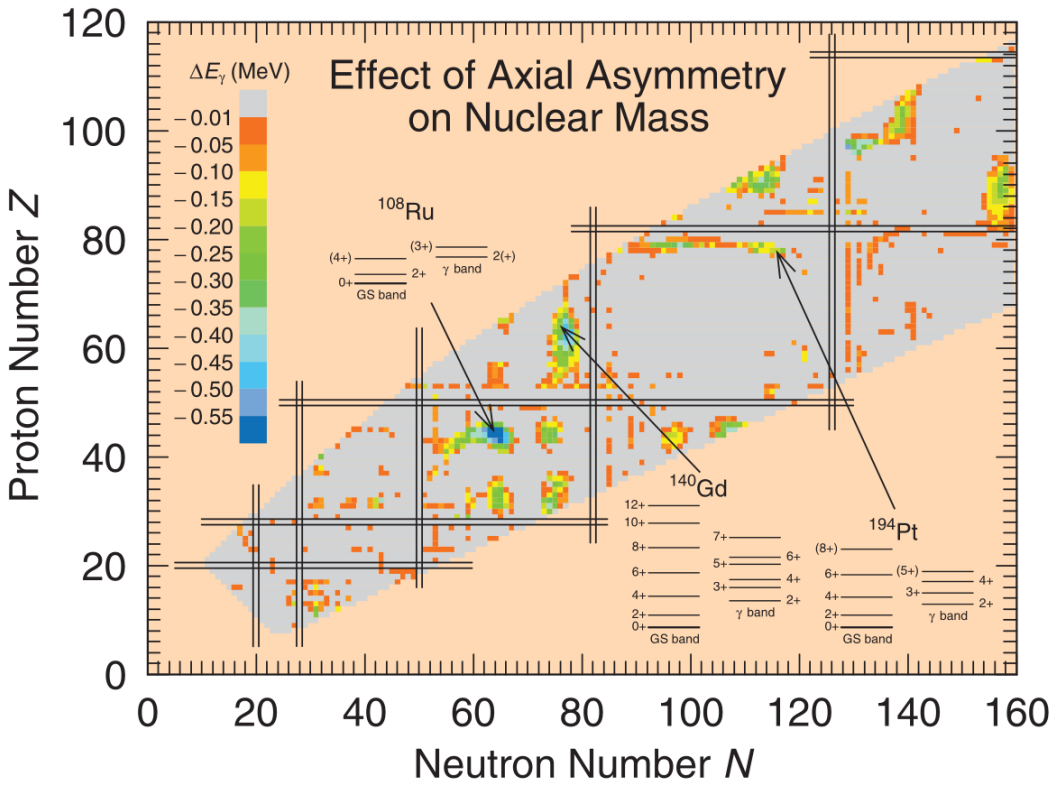

Figure 1.3 Calculated reduction in the nuclear ground-state energy when axial symmetry is broken relative to calculations limited to axially symmetric shapes only [13].

The degree of triaxiality introduced into the system depends upon the position of the Fermi surface of neutrons within the $h_{11/2}$ orbitals. Because of these, interesting shape

evolutions as a function of excitation energy, angular momentum, and particle number are expected in this region.

Triaxial nuclei have gained significant attention in recent years in nuclear physics; it is a very rare phenomenon and is predicted for the ground state of only a few small regions across the nuclear chart [13]. M*ö*ller *et al*. studied the influence of axial asymmetry on the ground-state mass of 5900 nuclei ranging from $A \approx 31$ to $N \approx 160$. Their results are displayed in Fig. 1.3, which illustrates the decrease of the nuclear ground-state energy when axial asymmetry is introduced in comparison to the axial symmetry shape. In Fig. 1.3, the blue color regions represent the observation of well-established triaxiality. A triaxial nucleus can manifest in various exotic band structures, and different quantum mechanical symmetries can be studied. The rotational band of an odd-*A* triaxial nucleus gets modified in a way such that the signature splitting ("signature" is a quantum number related to the symmetry of the rotation of a deformed nucleus by rotation π) becomes large even for a strongly coupled band with high-Ω configuration. In this thesis work, some of these exotic excitations that result from non-axial nuclear shape are mainly investigated. The non-axial or triaxial nuclear shape in atomic nuclei is manifested in the different types of excitations, which are listed in the following subsections.

1.1 γ - Vibrational Band

The vibrational states in deformed nuclei are of two types: β vibrations and γ vibrations. In the case of β vibration, axially symmetric vibration occurs, which appears as $K = 0_2$ state along with the ground state rotational band $K = 0_1$. The second vibration is based on the axially asymmetric vibration of the nuclear core with $K = 2$ projection on the symmetry axis, known as the γ vibration band. According to the rigid rotor model, the rotation of the rigid asymmetric nucleus not only yields ground state rotational band but also 2^+, 3^+, 4^+, 5^+,..... levels, generally known as anomalous rotational band or γ–band.

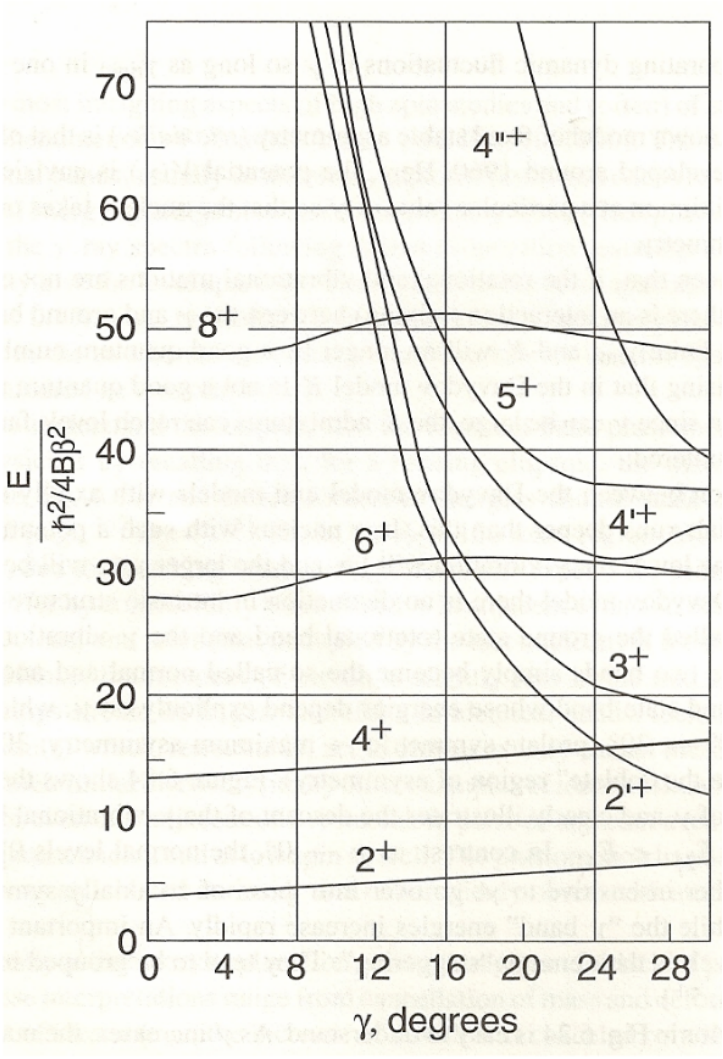

Figure 1.4 Calculated energy levels of a γ band using Davydov model.

According to Toki and Faessler, when the asymmetry parameter is low ($0^\circ < \gamma < 15^\circ$), the γ-band is a single rotational band. As the asymmetry parameter γ increases, the gamma band splits into two parts: one with even spin members and another with odd spin members. The second excited state of spin 2 (2_2^+) comes down in energy as the degree of non-axiality parameter γ increases towards maximum triaxiality of $\gamma = 30^\circ$ (see Fig. 1.4)[14, 15].

Experimental signature of γ - vibrational band

• The γ vibrational band and ground state band should have the same type of alignment and moment of inertia as a function of spin.

• Both the even and odd members of the gamma band decay to the ground state band through ΔI = 0,2 (even members) and 1 (odd members) transitions via $M1$+$E2$ mixed and $E2$ transitions.

Multiphonon deformed vibrations such as $\beta\beta$ ($K = 0$) vibration, $\beta\gamma$ ($K = 2$) vibration, and $\gamma\gamma$ ($K = 0$ and $K = 4$) vibration are also possible. However, the quasi-particle-phonon nuclear model (QPNM) has predicted that there would be no two-phonon states in even–even deformed nuclei because of the Pauli principle. The multi-phonon method (MPM) [16], the extended interacting-boson model (sdg-IBM) [17], and the self-consistent collective-coordinate method (SCCM) [18] have predicted the existence of $\gamma\gamma$ states in even-even deformed nuclei. They predicted that the $\gamma\gamma$ states have large anharmonicity. The energies of the $\gamma\gamma$ states should be around a factor ~ 2.6 times those of the γ states, and the transitions from the $\gamma\gamma$ to the γ bands should be consistent with their collective properties. The experimental observation of multi-phonon vibrational bands is very difficult due to their highly non-yrast nature and similar band head excitation energies as those of the 2-qp band. The decay transitions from the $\beta\beta$ ($K = 0$), $\beta\gamma$ ($K = 2$), and $\gamma\gamma$ ($K = 0$ and $K = 4$) to the ground state band, and also for $\gamma\gamma$ to $\beta\beta$ are forbidden.

The gamma vibrational band has been observed in many nuclei in different mass regions. For example: ^{103,104,105,106,108}Mo [8, 9, 19], ^{108,112}Ru [20], ^{103}Nb, ^{107,109}Tc [21, 22] ^{186,188}Os [23, 24] and ^{114}Te [25]. In all these nuclei, multiphonon excitations ($\gamma\gamma$) have also been reported.

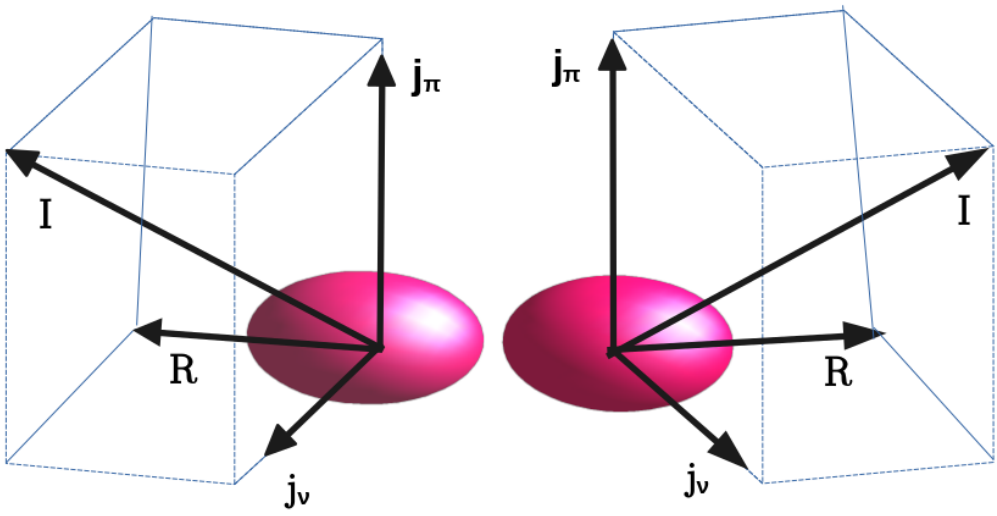

Figure 1.5 Geometrical representation of chiral configuration in a nucleus.

1.2 Chiral Rotation

The degenerate chiral doublet band was first predicted by Frauendorf and Meng [26] in the stable triaxial nucleus. Figure. 6.13 depicts how the chiral partner bands originate in triaxial nuclei. A high-$\boldsymbol{j}$ particle aligns its angular momentum $\boldsymbol{j}_p$ along a short axis (s). In this situation, there will be maximal overlap between the triaxial core and the density distribution of the particle, which helps in the minimization of attractive short-range core-particle interaction. Likewise, the high-$\boldsymbol{j}$ hole aligns its angular momentum $\boldsymbol{j}_h$ along the long (l) axis because in this orientation the overlap between the density distribution of the hole and the triaxial core will be minimal, which results in minimization of the repulsive short-range core-hole interaction. The angular momentum of the even-even core $\boldsymbol{R}$ is of a collective nature; it orients along the intermediate axis, which has the largest moment of inertia because it has the maximum deviation from the symmetry axis [27]. The total angular momentum $\boldsymbol{I}$ does not lie in any of the planes of the three angular momentum vectors $\boldsymbol{j}_p, \boldsymbol{j}_h$ and $\boldsymbol{R}$. The right-handed and the left-handed systems can be transformed

into each other by a combined operation of time reversal and rotation by 180° (TRy(π)) symmetry. For molecules, space inversion changes the left-handed configuration into a right-handed configuration, whereas for the triaxial nucleus, time reversal transforms the left-handed configuration into a right-handed configuration because angular momentum is an axial vector, which is invariant under space inversion and changes sign under time reversal.

Experimental signature of chiral symmetry broken

• Observation of two nearly degenerate $\Delta I = 1$ bands of the same parity and spin based on the same configuration.

• Both the double degenerate bands will exhibit similar properties, *i.e.*, very similar types of excitation energies, moments of inertia ($\mathscr{J}$), alignment, and electromagnetic properties like B($M1$)/B($E2$) ratio.

• For the doubly degenerate chiral bands, the electromagnetic transition strengths B($M1$) and B($E2$) as a function of spin should be very similar.

A large number of nuclei have been found to exhibit chiral symmetry breaking in different mass regions. For example, in mass region A≈80, chiral doublet bands and multiple chiral double bands (M$_\chi$D) have been reported in the many Br and Kr isotopes [28–32] based on proton and neutron $g_{9/2}$ orbitals. Similarly, this phenomenon is observed in another mass region A $\approx$ 100 (^{104}Rh [33], ^{105,107,108}Ag [34–36]), A $\approx$ 130 (^{135}Nd [37], ^{134}Pr [38], ^{124,126,128}Cs [39–41], ^{133}Ce [42]), and A$\approx$ 190 (^{188}Ir [43], ^{195}Tl [44]) based on high-j configurations. Recently, multiple chiral doublet bands, based on 3-qp and 5-qp configurations, have been observed in ^{195}Tl [44] nucleus. A small observed energy difference between the chiral partners indicates rapid conversion between the left-handed and right-handed configurations (**chiral vibration**). As the energy decreases between the chiral partner bands with an increase in spin, the left-right mode changes from soft

chiral vibration to well-established chiral configurations (**static chirality**). The ^{135}Nd [37] nucleus based on 3-qp ($\pi h^2_{11/2} \nu h^1_{11/2}$) was reported to show a transformation from chiral vibration to static chirality.

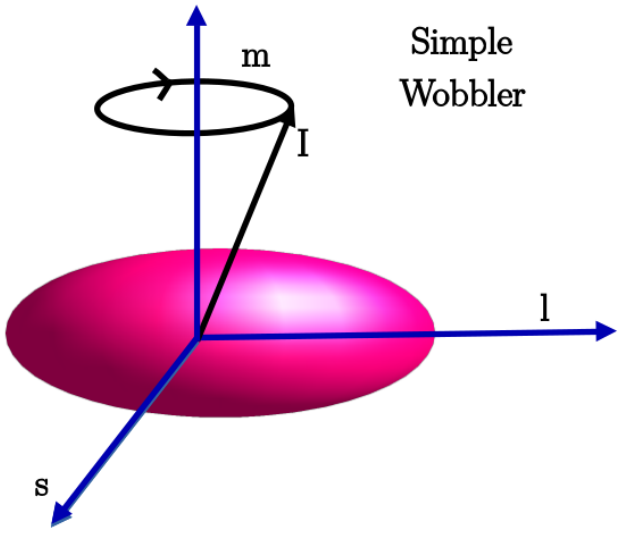

Figure 1.6 Geometrical representation of simple wobbler in even-even nucleus.

1.3 Wobbling Motion

This exotic motion was first predicted by Bohr and Mottelson in an even-even triaxial nucleus [45], which is analogous to the classical rotation of an asymmetry top (see Fig. 1.6). It is defined as the harmonic oscillation of one of the three principal axes of a triaxial rotor about its total angular momentum vector, which is spatially fixed. A triaxial nucleus has different moments of inertia along long (l), short (s), and medium (m) axes, and the nucleus tries to rotate around a medium axis (largest moment of inertia) to minimize its rotational energy. In Fig. 1.7, the variation of the moment of inertia along different axes with respect to γ has been shown for irrotational flow and the cranking model [46]. If $0^\circ < \gamma < 30^\circ$, then the m-axis is closer to that of the s-axis, and it has a larger moment of inertia than the l-axis. If $30^\circ < \gamma < 60^\circ$, then the m-axis is closer to that of the l-axis, and

it has a larger moment of inertia than the s-axis. A number of wobbling bands have been reported in the mass region A≈ 180(^{187,183}Au [47, 48]), 160 (^{161,163,165,167}Lu [49–52]), 130 (^{125,127}Xe [53, 54], ^{130,133}Ba [55, 56], ^{133}La [57], ^{136}Nd [58], ^{135}Pr [59]), 100 (^{105}Pd [60], ^{112}Ru [61]), and 80 (^{74}Br [62]).

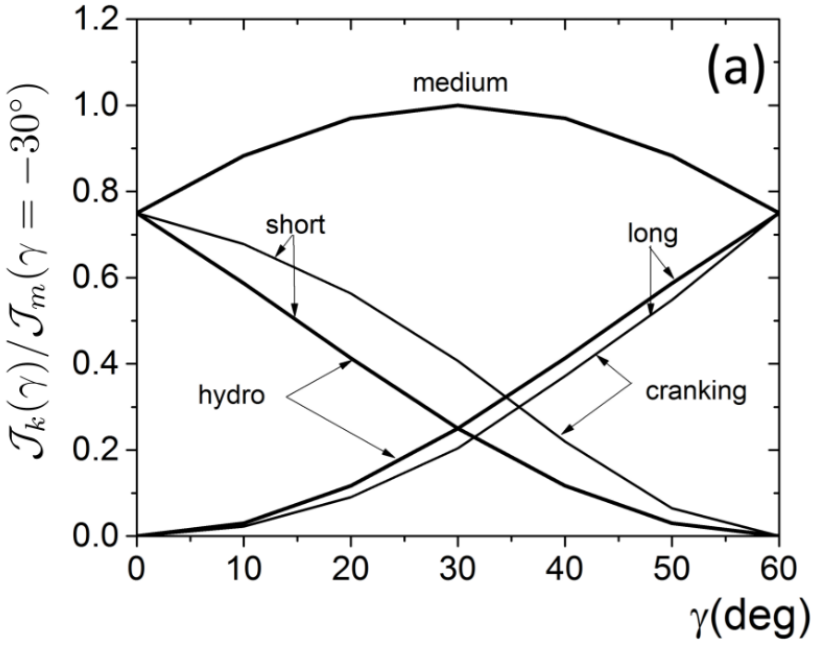

Figure 1.7 The moments of inertia of the three principal axes as a function of the triaxiality parameter γ. The term "hydro" denotes the irrotational flow values and "cranking" the cranking values, which are scaled by the factor $\mathcal{J}_m^{hyd}(\gamma)/\mathcal{J}_m^{crank}(\gamma)$ [46].

Depending on the coupling of an odd particle with the triaxial core [63], two different types of wobbling motion (see Fig. 1.8) are observed in the case of odd-A nuclei

- Longitudinal wobbling
- Transverse wobbling

In the case of longitudinal wobbling, the angular momentum of the odd particle aligns along the middle axis (m), and wobbling energy increases as a function of spin. While it aligns along the long or short axis for transverse motion, where the decreasing nature of

wobbling energy is observed as a function of spin. In the case of odd-A nuclei, there exists a signature partner band along with a wobbling band with large signature splitting [63], which arises when the angular momentum of the odd particle aligns away from any of the principal axes.

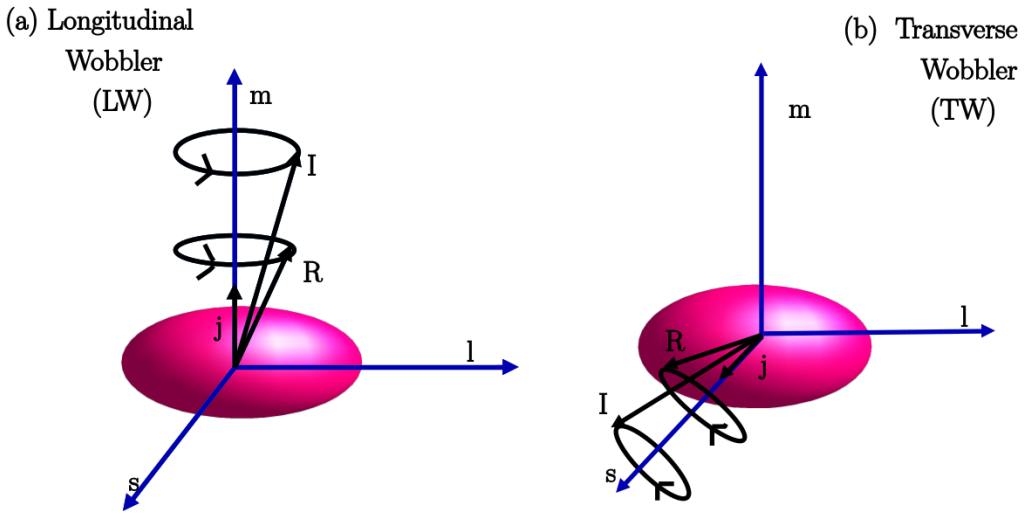

Figure 1.8 Pictorial representation of longitudinal and transverse wobbling motion in odd-A nucleus.

The experimental signature of this exotic mode is the observation of multiple rotational bands, each corresponding to a particular phonon number (n_ω) with the following properties:

• Each rotational bands are connected by $\Delta I = 1$ interconnecting transition.

• This phenomenon has a collective nature, so each $\Delta I = 1$ transition should have a predominant $E2$ character (*i.e.*, a large value of mixing ratio).

• The reduced transition probability ratio of the interband to intraband $E2$ transitions, *i.e.*, $\mathrm{B}(E2)_{out}/\mathrm{B}(E2)_{in}$ is large.

In addition to the above exotic modes, which have been discussed in the above section, the nucleus can have a pear-like shape *i.e.*, octupole-deformed shape. The static octupole

deformed nucleus shape $Y_{3,\mu}$ breaks the symmetry of the reflection on a plane that depends on μ [64]. For a $Y_{3,0}$ octupole shape, the properly interleaved positive and negative band is observed with spin and paries of $I_\pi = 0^+, 1^-, 2^+, 3^-, 4^+, 5^-, \ldots$. Since, the value of $Y_{3,0}$ is finite at zero deformation so it lowers the positive parity states with respect to the negative states. The manifestation of this phenomenon is discussed in the section below:

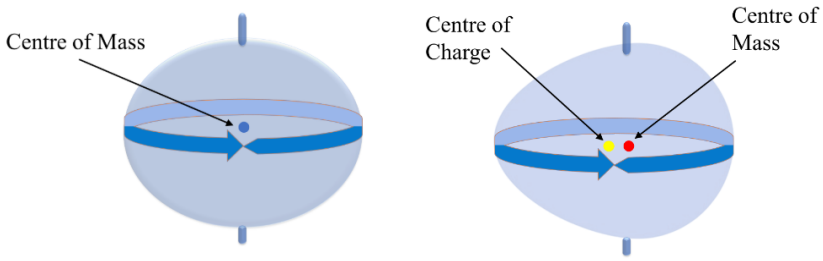

Figure 1.9 Pictorial representation of the difference in center of mass and center of charge distribution.

1.4 Reflection Asymmetry Shape

The reflection asymmetric shape arises when occupancy of nucleons leads to the deviation of charge and mass distribution from spherical symmetry, as shown in Fig. 1.9, the resultant shape is generally known as the octupole shape or pear shape. This phenomenon occurs when nucleons near the Fermi surface occupy the states of opposite parity with $\Delta l = \Delta j = 3$ ($p_{3/2}$ and $g_{9/2}$, $d_{5/2}$ and $h_{11/2}$, $f_{7/2}$and $i_{13/2}$, $g_{9/2}$ and $j_{15/2}$). The sequence of negative-parity states which are connected to the positive-parity states via strong $E1$ transitions is interpreted as a strong signature of reflection asymmetry shape. Theoretical calculation predicts octupole deformation to be more prominent in nuclei having N (neutron number) 34, 56, 88, 136, which is experimentally supported by the observed octupole correlation in Ra, Th ($Z \approx 88$, $N \approx 136$) [65, 66], Ba ($Z \approx 56$, $N \approx 88$) [67, 68] and Ge($Z \approx Z \approx 32$) [69] isotopes. The octupole correlations are of two types: static or dynamic (vibrational),

and it has also been proposed that nuclei having dynamic octupole deformations at low spin could acquire static octupole deformations at high spin. In the case of static deformation, the nucleus cannot form a reflection-symmetric shape due to the presence of an infinite barrier between the two minima at β_3. In this case, both the positive and negative parity states are perfectly interleaved with each other. In octupole vibration, the two minima in the potential energy at $\pm\,\beta_3$, are separated by a small barrier. In this situation, the nucleus can tunnel through the barrier and take the reflection symmetric shape, causing parity splitting between the positive- and negative-parity states (see Fig. 1.10).

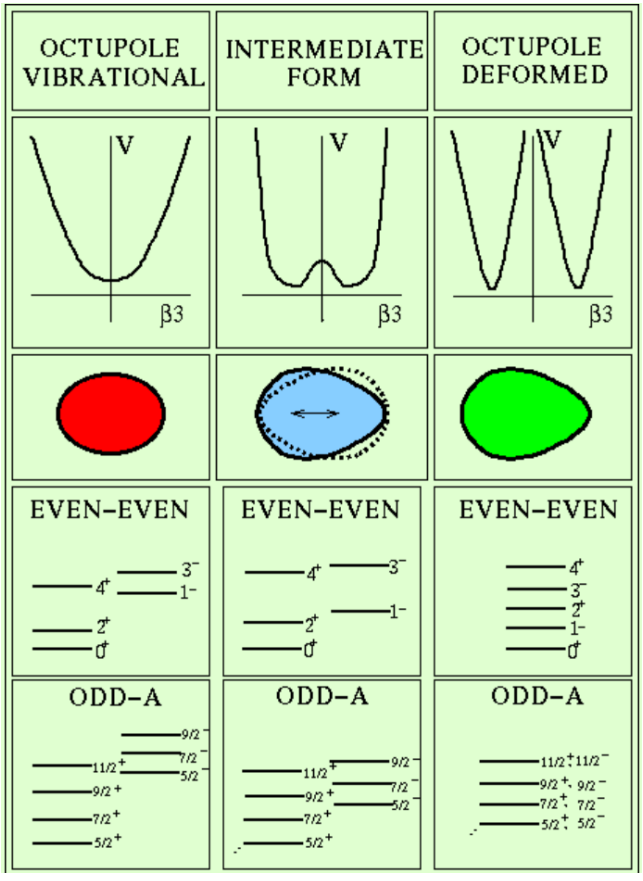

Figure 1.10 Potential energy surface plot with respect to β_3 for octupole vibration and octupole deformed shape [70].

Theoretically, the enhanced octupole strengths at high spin can be expected to depend on two factors: the increased mixing between single-particle states of opposite parity orbitals that approach each other with increasing rotational frequency and a larger moment of inertia at the octupole shape due to weaker pairing correlations. There are two parameters that decide the degree of octupole deformation in a nucleus:

• The ratio of rotational frequency between the positive and negative parity bands should be 1.

• The energy difference between the positive and negative parity bands should tend to zero as the spin increases.

Both parameters measure the extent of interleaving between the positive and negative-parity states. The observed B($E1$) strength should be of the order of 10^{-4} e^2fm^2.

With the aim to observe different manifestations of triaxial shapes and their coupling with the odd-particles, the excited states in three nuclei, namely, ^{125}Xe, ^{114}Te, and ^{119}I have been experimentally studied in this thesis work using the in beam gamma-ray spectroscopy technique.

1.5 Outline of the Thesis

The present thesis has been arranged in seven chapters:

Chapter 1: Introduction: A brief introduction to the evolution of shapes, especially triaxial and reflection-asymmetric shapes, has been presented. The phenomena associated with these shapes are discussed extensively based on various experimental observations in different mass regions $A \approx 80$, 100, 130, and 180.

Chapter 2: Experimental Techniques and Data Analysis: Chapter 2 summarizes the details of the experimental instrumentation which have been used to populate the desired nuclei. The γ spectroscopy studies were performed by using the Gammasphere array

and Indian National Gamma Array (INGA) spectrometers located at Argonne National Laboratory (US), TIFR (India), and VECC (India), respectively. High-spin states in nuclei were populated through fusion-evaporation reactions. Data analysis was performed by using Gammasort, INGASort, MARCOS code, and Radware software. The spin and parity of the excited states have been ascertained through angular distribution ratio, direction correlation ratio, and polarization measurements.

Chapter 3: Nuclear Models: This chapter briefly summarizes nuclear models such as spherical and deformed shell model, collective behavior of nuclear motion, cranking model, triaxial projected shell model, covariant density functional theory, ultimate cranking theory, and large-scale shell model calculation for understanding nuclear structure.

Chapter 4: Possible Wobbling Phenomenon in ^{125}Xe: The negative-parity bands based on the $\nu h_{11/2}$ configuration in ^{125}Xe have been revisited. Evidence for first and second-phonon wobbling excitations has been established by measurements of directional correlation ratios and angular distributions of the involved γ rays. The observed wobbling energy of the bands involved was compared within the framework of triaxial projected shell-model calculations.

Chapter 5: Evolution of Quadrupole and Octupole Excitations beyond Noncollective States in ^{114}Te : The previously known level structure of ^{114}Te has been extended by adding 35 newly observed γ transitions. The spin and parity of newly observed γ-transitions were confirmed by directional correlation ratio and polarization measurements. Furthermore, the presence of octupole correlation is verified in this nucleus through the presence of several enhanced $E1$ transitions. To explore the observed structure of ^{114}Te, the KSHELL code within the framework of the Shell model, Covariant density functional theory, and the Ultimate cranking model were used.

Chapter 6: Observation of Transverse Wobbling Motion and Chiral Bands in ^{119}I: The negative parity states of this nucleus are based on $\pi h_{11/2}$ orbitals. Observation of a

large $E2$ fraction of the interconnecting transitions decaying from the previously reported unfavored signature partner band to the yrast band indicates the presence of wobbling motion in ^{119}I. A pair of chiral doublet bands is also observed with negative parity. The observed variation of excitation energies, staggering parameter, and B($M1$)/B($E2$) ratios with respect to spin shows a similar type of behavior in both bands, which is the signature of the chiral partner's band.

Chapter 7: Conclusions and Scopes of Future Work: The chapter summarizes the overall findings and observations as well as discusses future scopes in the context of the present thesis.